REPORT DOCUMENTATION PAGE

Form Approved
OMB No. 0704-0188

1. AGENCY USE ONLY *(Leave Blank)*	2. REPORT DATE	3. REPORT TYPE AND DATES COVERED
	24 June 1999	10/98-9/99

4. TITLE AND SUBTITLE
Ionization of Thin and Thick Water Films on Platinum Field Emitter Tips – A Comparison of Theoretical and Empirical Trends

5. FUNDING NUMBERS
N00014-97-1-0417

Richard Carlin

6. AUTHOR(S)
D. L. Scovell, T. D. Pinkerton, V. K. Medvedev, and E. M. Stuve

7. PERFORMING ORGANIZATION NAME(S) AND ADDRESS(ES)
University of Washington
Department of Chemical Engineering
Box 351750
Seattle, WA 98195-1750

8. PERFORMING ORGANIZATION REPORT NUMBER
Technical Report No. 12

9. SPONSORING / MONITORING AGENCY NAME(S) AND ADDRESS(ES)
Office of Naval Research
800 N. Quincy Street
Arlington, VA 22217

10. SPONSORING/MONITORING AGENCY REPORT NUMBER

11. SUPPLEMENTARY NOTES
Prepared for publication in the Journal of Chemical Physics

12a. DISTRIBUTION / AVAILABILITY STATEMENT
This document has been approved for public release and sale; its distribution is unlimited.

12b. DISTRIBUTION CODE

13. ABSTRACT *(Maximum 200 words)*

Field ionization of thin water layers adsorbed onto a platinum field emitter tip was investigated by numerical simulation and analysis of experimental data. The numerical simulation, which includes a field-dependent relative permittivity, was developed to predict the field distribution around a water-covered field emitter tip. The simulation predicts that ionization begins at the water-vacuum interface in thin layers and at the tip-water interface in thick layers. Experiments were conducted to verify the predicted trends. Water was vapor deposited onto a cryogenically cooled tip under field-free conditions. Field ionization was probed by ramped field desorption (RFD) in which desorption of ionic species (hydrated protons) is measured while increasing the applied electric field linearly in time. The ionization onset field decreased from 0.5 to 0.2 V/Å as temperature increased from 105 to 150 K. The estimated average relative permittivity for crystalline ice is 2.5 and that of amorphous ice is 2.0. The experimental results are consistent with the trends predicted by the numerical model. Data at all temperatures show a change in slope when the water thickness exceeds a critical thickness. This change in slope is evidence of a change in ionization location. The measured slope agrees with the predicted slope for thin crystalline layers, but not for amorphous layers. Thinning of the amorphous layers due to field-enhanced mobility of the ice may explain the discrepancy with the model.

14. SUBJECT TERMS
Water, Field ionization, Platinum, Water ionization, Electric field effects, Dielectric properties

15. NUMBER OF PAGES
40

16. PRICE CODE

17. SECURITY CLASSIFICATION OF REPORT	18. SECURITY CLASSIFICATION OF THIS PAGE	19. SECURITY CLASSIFICATION OF ABSTRACT	20. LIMITATION OF ABSTRACT
Unclassified	Unclassified	Unclassified	

OFFICE OF NAVAL RESEARCH

Research Contract N00014-97-1-0417

Program Manager Richard Carlin

Technical Report No. 12

"Ionization of Thin and Thick Water Films on Platinum Field Emitter Tips – A Comparison of Theoretical and Experimental Trends"

by

D. L. Scovell, T. D. Pinkerton, V. K. Medvedev,
and E. M. Stuve

Prepared for Publication

in

Journal of Chemical Physics

University of Washington
Department of Chemical Engineering
Box 351750
Seattle, WA 98195-1750

June, 1999

Ionization of Thin and Thick Water Films on Platinum Field Emitter Tips – A Comparison of Theoretical and Empirical Trends

Dawn L. Scovell, Tim D. Pinkerton, Valentin K. Medvedev, and Eric M. Stuve*

University of Washington

Department of Chemical Engineering

Box 351750

Seattle, WA 98195

Submitted to: Journal of Chemical Physics

Date: 11 June 1999

ABSTRACT

Field ionization of thin water layers adsorbed onto a platinum field emitter tip was investigated by numerical simulation and analysis of experimental data. The numerical simulation, which includes a field-dependent relative permittivity, was developed to predict the field distribution around a water-covered field emitter tip. The simulation predicts that ionization begins at the water-vacuum interface in thin layers and at the tip-water interface in thick layers. Experiments were conducted to verify the predicted trends. Water was vapor deposited onto a cryogenically cooled tip under field-free conditions. Field ionization was probed by ramped field desorption (RFD) in which desorption of ionic species (hydrated protons) is measured while increasing the applied electric field linearly in time. The ionization onset field decreased from 0.5 to 0.2 V/Å as temperature increased from 105 to 150 K. The estimated average relative permittivity for crystalline ice is 2.5 and that of amorphous ice is 2.0. The experimental results are consistent with the trends predicted by the numerical model. Data at all temperatures show a change in slope when the water thickness exceeds a critical thickness. This change in slope is evidence of a change in ionization location. The measured slope agrees with the predicted slope for thin crystalline layers, but not for amorphous layers. Thinning of the amorphous layers due to field-enhanced mobility of the ice may explain the discrepancy with the model.

I. INTRODUCTION

High surface electric fields are the driving force behind many important processes, such as electrochemistry, corrosion, and field emission. Fields on the order of 1 V/Å are strong enough to make and break chemical bonds. The behavior of water in these fields is important because water is the primary component in electrochemical and corrosion processes as well as a major contaminant in the vacuum around field emitter arrays in flat panel displays. It is usually assumed that water amplifies the field at electrode surfaces[1], but little is actually known about how water affects the electric field distribution. In a previous modeling study we predicted that the field is concentrated at metal surfaces covered by thick water layers and that it is concentrated at the water/vacuum (or air) interface when the water layer is thin[2].

Field emitter tips lend themselves to the study of electric field effects in water because, unlike planar electrodes, they allow independent control of very large electric fields. Ionization of water deposited onto a field emitter tip will depend upon the morphology of the water layer[3,4]. Multilayers of water can be vapor deposited on cryogenically cooled emitter tips. The water deposited under these conditions is either amorphous ice, crystalline ice, or a mixture thereof. The structure of the ice layer depends upon the surface temperature, deposition rate[5-10], and the wettability of the surface[11]. Three phases of water can exist below 160 K: an amorphous solid, a highly viscous fluid, and a crystalline solid.

Two temperatures are of particular interest when discussing properties of vapor deposited water: the glass transition temperature T_g and the crystallization temperature. The glass transition temperature for vapor-deposited amorphous ice is 115 – 140 K[12-15]. The glass transition temperature is the temperature at which vapor deposited water changes from an

amorphous solid to a highly viscous fluid[12]. The protons are frozen in the amorphous solid and mobile in the highly viscous fluid, allowing configurational rearrangement of the hydrogen network through molecular rotation and through formation and transfer of Bjerrum defects[10]. Experimental results have shown that the highly viscous fluid has translational mobility. Temperature programmed desorption (TPD) studies of the isotopic mixing of water films show that large scale translational motion occurs between the glass transition temperature and below the crystallization temperature[16]. Large scale translational diffusion of the fluid has also been observed with transmission electron microscopy[17]. At the crystallization temperature the highly viscous fluid transforms into a crystalline solid.

The temperature dependence of field ionization of vapor deposited water on field emitter tips was investigated in a previous study[4]. Ionization of water below 130 K was distinctly different from that above 130 K, due to a phase change in the water layer. Water below 130 K was assumed to be amorphous and that above 130 K crystalline. This phase change occurred approximately 20 K lower than that of pure amorphous ice[18]. The presence of crystalline nuclei, along with the ordering influence of the applied electric field, were attributed to the reduction of the crystallization temperature from the expected value[4].

In this paper we report additional results for the field ionization of water. Water was adsorbed at temperatures of 100 to 150 K onto a platinum field emitter tip under field-free conditions in ultrahigh vacuum. The effects of temperature, ice thickness, and potential ramp rate on the ionization of water were studied in two series of experiments. The first characterized ionization onset as a function of temperature and ice thickness. The second series of experiments measured the effect of varying the potential ramp rate on the onset of ionization at different

thicknesses and temperatures. We interpret the results in terms of the structure, ionization location, and thickness dependence of the field at ionization onset and compare the experimental results with those of a previous modeling study[2].

II. EQUIPMENT AND PROCEDURE

The experimental apparatus and procedure have been described previously[19] and will therefore be described only briefly. The vacuum chamber was pumped by a turbo-molecular pump and titanium getter pump to obtain a base pressure of 10^{-10} torr. A field emitter tip was used to generate electric fields as large as 4 V/Å. Ions produced by the tip were projected onto a pair of chevron microchannel plates (MCP) and directed onto a phosphor screen to form a greatly magnified, projection image of the tip surface. This image shows the detailed atomic arrangements of the hemispherical tip surface[20]. Field ionization images were recorded with a CCD camera and VCR.

A platinum tip, oriented along the [100] axis, was spot-welded to a 0.25 mm diameter heating loop mounted to the bottom of a cryogenically cooled downtube. The temperature was measured by a chromel/alumel thermocouple spot-welded to the heating loop. The desired temperature was maintained within ± 0.3 K by a PID temperature controller connected to a d.c. power supply for resistive heating. A high voltage feedthrough at the bottom of the downtube provided high voltage isolation for the heating loop/tip assembly.

The field emitter tip was electrochemically etched from 0.013 mm diameter platinum wire at 2-3 V d.c. in a molten mixture of sodium chloride and sodium nitrate. The tip radius was determined from the best imaging field of 3.75 V/Å for neon[21]. The relationship between the applied potential V_t and the applied field F_{app} is

$$F_{app} = V_t / \beta r_t , \quad (1)$$

where β is the shape factor and r_t is the tip radius. The shape factor is 5 for a typical emitter tip[22]. The tip radius in these experiments ranged from 335 to 374 Å. Tip radii determined from the best imaging field were within 20% of those estimated by counting the number of lattice steps between the (001) and (113) planes in the field ionization images. The relative error in the electric fields reported in these experiments is less than 5%. In this paper the term "applied field" is used to describe the field that would occur at a bare tip surface in vacuum for a given applied tip potential.

A three-step procedure was used to ensure that the tip was free from contaminants at the beginning of each experiment. First, the tip was heated to 500 K to desorb water from the tip and heating loop assembly. Second, any remaining contaminants were field desorbed from the tip by imaging in neon and hydrogen. Finally, a small amount of platinum was field desorbed in neon to ensure that the surface was atomically clean.

Prior to dosing, water was degassed with both liquid nitrogen and dry ice in several freeze-thaw cycles. Water was introduced into the background of the vacuum chamber through a variable leak valve to produce a uniform layer of ice on the tip under field-free conditions. The tip was held at the desired temperature during dosing. The tip was exposed to 5.0×10^{-7} torr of water for 2 to 60 minutes. Chamber pressures of less than 5.0×10^{-9} torr were typically achieved within 2 to 10 minutes after dosing. The deposition rate was ~0.8 Å/s under these conditions. Water thicknesses of 50 to 3600 Å were obtained in these experiments.

The water layer thickness was estimated from the empirical method developed by Brown

et. al.[23]. The maximum growth rate of the water layer is determined by the incident flux J_{in}:

$$J_{in} = \frac{P_w}{N_w\sqrt{2\pi mkT_g}} \tag{2}$$

where P_w is the partial pressure of water, N_w the surface density of a monolayer of water, m the mass, k Boltzmann's constant, and T_g the gas temperature. The surface density of a monolayer of water is $1.056\text{x}10^{15}$ molecules/cm^2/ML[23]. It is necessary to correct the growth rate by the desorption flux J_{des}:

$$J_{des} = \nu_o \exp\left[\frac{-E_d}{kT_s}\right] \tag{3}$$

where ν_o is the desorption pre-exponential factor of $4\text{x}10^{15}$ ML/s, E_d the desorption activation barrier of 48.25 kJ/mol[23], and T_s is the surface temperature. The condensation coefficient for the water layer is defined as:

$$\alpha = S(T) - \frac{J_{des}(T)}{J_{in}} \tag{4}$$

where $S(T)$ is the sticking coefficient. The sticking coefficient for water is 1.0 below 160 K[23]. The thickness of water on the surface is the difference between the amount of water deposited during deposition and the amount of water leaving the surface during chamber pump down:

$$t_w = \frac{M}{\rho N_A}\left(\frac{\alpha P_w}{\sqrt{2\pi mkT_g}}\tau_{exp} - J_{des}N_w\tau_{pump}\right) \tag{5}$$

where M is the molecular weight, ρ the density of the water adlayer, N_A Avagadro's number, τ_{exp} the exposure time, and τ_{pump} the pump down time. The second term in Eqn. 5 is very small at temperatures less than 145 K. The density of the water layer varies linearly from 0.8 g/cm^3 at 80 K to 0.93 g/cm^3 at 130 K[23].

Ramped field desorption (RFD) spectra were obtained after removing water from the background gas[24]. During the RFD runs, the potential applied to the tip was increased at a constant rate. When the field becomes sufficiently large, ions are created, desorb from the water layer, accelerate away from the tip radially, and detected at the MCP/phosphor screen assembly. The signal from the phosphor screen was monitored by two rate meters, each with a time constant of 0.1 s. The first rate meter was always set to a sensitivity of 300 counts per second (CPS) full scale, while the second was adjusted to capture the entire peak. The first rate meter was used to determine ionization onset.

III. RESULTS

A. Temperature and Thickness Dependence

The effects of temperature and ice thickness on the ionization of water were studied in two series of experiments. The first characterized ionization onset as a function of temperature and ice thickness. The ionization onset field $F_{app,o}$, defined experimentally as the applied field at which ionization reaches 10 counts/s, was measured as a function of the dimensionless ice thickness at temperatures between 100 and 150 K. The dimensionless thickness x is the ratio of the thickness of the ice layer to the tip radius. The ionization threshold of 10 counts/s is lower than used previously[19] as a result of lower background noise levels in these experiments. The first

series of RFD experiments was conducted at a potential ramp rate of 10 V/s, which corresponds to an applied field ramp rate of 6 $mV\text{Å}^{-1}s^{-1}$. Fig. 1 shows the dependence of the onset field on thickness at 143 K. The data fall on two lines. The solid dots in Fig. 1 were used to determine the thin coverage line ($x < 0.8$). In this study, thin layers are defined as points that fall below the change in slope (slope break) and thick layers as those that lie above the slope break. Near the slope break there is a transition region in which the ionization phenomena are mixed. The slope break was present at all temperatures examined.

A CCD camera and VCR recorded ionization images on the phosphor screen during each run. The images for thin layers were distinctly different than those for thick layers at all temperatures. Ionization images for thin layers were diffuse and sporadic, while for thick layers the images ended in a flash, for temperatures less than 130 K, or had highly localized, persistent ionization zones for temperatures greater than 130 K[4]. Both the presence of a slope break in plots of onset field as a function of thickness (Fig. 1) and the thickness dependence of the ionization images indicate that different ionization mechanisms occur in thin layers versus thick layers of water.

The slope $dF_{app,o}/dx$ below the slope break (i.e., for thin coverage) is strongly dependent upon temperature. Fig. 2 shows an expanded view of the thin coverage data at 108 K. The slope of this data is considerably less than the slope of the 143 K data in Fig. 1. The differences in the slopes above and below 130 K are readily apparent in Fig. 3, which shows the temperature dependence of $dF_{app,o}/dx$ for thin layers of water. The open circles are the experimental data. Below 130 K, $dF_{app,o}/dx$ is approximately 0.1 V/Å and above 130 K it ranges from 0.2-0.3 V/Å. The plotted slopes and error bars were determined by linear regression.

The field ionization images and spectra show that ionization in thin layers differs from that in thick layers. The slope break in plots of ionization onset $F_{app,o}$ as a function of thickness x (e.g., Fig. 1) indicate a change in ionization mechanism. Fig. 4 shows that the temperature dependence of the dimensionless thickness at the slope break x_c , falls gradually from 2.3 near 100 K to 1.7 near 130 K. At 130 K, the dimensionless thickness at the slope break drops abruptly to 1.0 and then gradually decreases to 0.5 at 148 K.

Extrapolation of the thin coverage lines in Figs. 1 and 2 to zero thickness gives an estimate of the actual field required to ionize the ice, F_o. Extrapolation is necessary to correct for screening of the field by water layers of finite thickness. The onset field F_o is a true, rather than applied, field because the influence of water layer thickness has been removed. The extrapolated onset fields are shown in Fig. 5. The onset field abruptly changes to a lower field at 130 K. The trend in the extrapolated onset field is linear above and below 130 K. In a previous study[4], the sudden changes at 130 K in slope, ionization onset field, and the ionization images were attributed to a phase change from amorphous to crystalline ice.

B. Ramp Rate Dependence

The effect of field ramp rate on ionization onset was investigated in a second series of experiments. The potential ramp rate was varied from 3 to 1000 V/s (applied field ramp rates from 2 to 600 $mV\text{Å}^{-1}s^{-1}$) for constant ice thicknesses at 108 K and 143 K (i.e., amorphous and crystalline ice). Fig. 6 shows the dependence of ionization onset on ramp rate at 108 K for dimensionless thicknesses of 0.7, 2.9, and 4.3. The triangles in Fig. 6 are thin layer data ($x = 0.7$) and the circles are thick layer data. Ionization onset is independent of ramp rate for thin layers.

In thick layers, the onset field $F_{app,o}$ initially increases with increasing ramp rate, but eventually reaches a plateau. The plateau begins at 40 $mV\text{Å}^{-1}s^{-1}$ for $x = 2.87$ and at 8 $mV\text{Å}^{-1}s^{-1}$ for $x = 4.26$. The onset field for the thickest layer depends more strongly upon ramp rate. The lines through the data assume that the onset field is linearly dependent upon ramp rate, and they appear as curves because of the semi-logarithmic plot.

Fig. 7 shows that the trends at 143 K are the same as those at 108 K. The data for the thin layer of ice ($x = 0.6$) are independent of ramp rate and the data for the thick layer of ice ($x = 2.4$) are linearly dependent on ramp rate up to 8 $mV\text{Å}^{-1}s^{-1}$. The slope of the 143 K data is approximately 50% greater than the slope at 108 K for approximately the same ice thickness: the 108 K data has a slope of 10.6 s for $x = 2.9$ while the 143 K data have a slope of 15.2 s for $x = 2.4$. The lower rate of change at 108 K indicates that ionization in amorphous layers is less sensitive to changes in applied field than the 143 K data.

The shaded rectangles in Fig. 1 show the range of ionization onset observed in the ramp rate studies at 143 K. Note that the range of the thin coverage data (i.e., the height of the rectangle at $x = 0.6$) is approximately the same as that of the constant ramp rate data (i.e., the solid circles) at the same thickness. In other words, the variation in the thin coverage data is within the experimental error of the constant ramp rate experiments. The range of ionization onset observed for the thick layer data at $x = 2.5$, on the other hand, is much larger than that of the constant ramp rate data at the same thickness. This variation is too great to be explained by normal statistical variation. This supports the finding that ionization in thin layers occurs by a different mechanism than ionization in thick layers. The ramp rate data show that ionization onset in thin layers is unaffected by changes in ramp rate, while in thick layers, ionization onset depends

upon ramp rate.

IV. DISCUSSION

The experimental data show that ionization in water films depends not only upon temperature, but also upon the thickness of the water adlayer. The temperature dependence can be explained by a phase change in the water adlayer, as discussed in a previous publication[4]. The thickness dependence and its implications for ionization mechanisms will be discussed below.

A. Thickness Dependence of Ionization Mechanisms

The applied field required to ionize the ice layer increases with increasing thickness. This is easily explained by dielectric screening of water; thicker water layers are more effective at screening the field at the water-vacuum interface. A more quantitative description of the thickness dependence can be obtained by comparing the experimental results with our previous modeling study of the field distribution in water adlayers. In this study, the effect of condensed water on the electric field distribution was calculated by assuming that: the tip can be approximated as a spherical, perfect conductor; water does not react with the substrate; macroscopic properties apply; and water ionization is negligible [2]. With these assumptions the potential V can be found by solving Poisson's equation

$$\frac{d^2V}{dr^2}+\left[\frac{2}{r}+\frac{1}{\varepsilon(F)}\frac{d\varepsilon(F)}{dr}\right]\frac{dV}{dr}=0 \qquad (6)$$

for the water layer and Laplace's equation

$$\frac{d^2V}{dr^2}+\frac{2}{r}\frac{dV}{dr}=0 \qquad (7)$$

for the vacuum outside the water layer, where r is radial distance from the origin, and ε the relative permittivity. The boundary conditions are:

(1) the potential at the tip surface: V_t,

(2) equality of potential at the water/vacuum interface: $V_w|_{r=r_w} = V_v|_{r=r_w}$,

(3) equality of electric displacement at the water/vacuum interface:

$$\varepsilon(F_w)\frac{dV_w}{dr}\bigg|_{r=r_w} = \frac{dV_v}{dr}\bigg|_{r=r_w}, \text{ and}$$

(4) zero potential infinitely far from the tip ($V_v|_{r=\infty} = 0$),

where the subscripts w and v refer to water and vacuum, respectively.

The difficulty of solving this set of equations depends upon the relative permittivity. If the relative permittivity is assumed to be constant, then the equations can be solved analytically. At high field strengths (i.e., those of interest in this work) the relative permittivity is not constant. However, the constant permittivity case is worth examining because it allows simple expressions to be derived for the fields at the tip/water and water/vacuum interfaces. As these expressions are useful in understanding the expected trends, the solution for the constant permittivity case will be discussed before the variable permittivity solution is presented.

1. Constant Relative Permittivity

For the constant permittivity case, Eqn. 6 simplifies to Laplace's equation (Eqn. 7). Note that relative permittivity is present only in the third boundary condition. The field at the vacuum

interface F_v can be determined by solving Laplace's equation:

$$F_v = \left.\frac{-\mathrm{d}V}{\mathrm{d}r}\right|_{r=r_w} = \frac{\varepsilon F_{app}}{(x+\varepsilon)(x+1)}. \tag{8}$$

where ε is the dielectric constant of the water layer and x the dimensionless thickness of the water layer

$$x = \frac{r_w - r_t}{r_t} = \frac{r_w}{r_t} - 1, \tag{9}$$

where r_w is with respect to the origin used to define r_t. Eqn. 8 predicts that the field at the vacuum interface will decrease with increasing water thickness.

The rate of change of the applied field with respect to the thickness, $\mathrm{d}F_{app}/\mathrm{d}x$, at constant F_v can be found by combining Eqns. 8 and 9 and then differentiating:

$$\frac{\mathrm{d}F_{app}}{\mathrm{d}x} = F_v\left(1 + \frac{2x+1}{\varepsilon}\right), \tag{10}$$

This expression predicts that the slope $\mathrm{d}F_{app}/\mathrm{d}x$ is always positive and that it approaches a minimum value of F_v as the relative permittivity approaches infinity (i.e., a perfect metal).

Similarly, the field at the tip surface F_t is:

$$F_t = \left.\frac{-\mathrm{d}V}{\mathrm{d}r}\right|_{r=r_t} = F_{app}\left(\frac{x+1}{x+\varepsilon}\right) \tag{11}$$

This equation predicts that the tip field will increase as the thickness of the water layer increases

for a given applied field and $\varepsilon>1$. The slope dF_{app}/dx at constant F_t can be found by rearranging and differentiating Eqn. 11:

$$\frac{dF_{app}}{dx} = F_t\left[\frac{1-\varepsilon}{(1+x)^2}\right], \tag{12}$$

This expression predicts that the slope is expected to be negative when $\varepsilon > 1$.

The above expressions predict that as the water thickness increases, the field at the tip surface will increase and the field at the vacuum interface will decrease. Therefore, there must be a critical thickness below which F_v dominates and above which F_t dominates. This critical thickness x_c can be determined by equating Eqns. 8 and 11:

$$x_c = \sqrt{\varepsilon} - 1. \tag{13}$$

This expression predicts that when the relative permittivity decreases the critical thickness will also decrease.

2. Variable Relative Permittivity

A more realistic field distribution can be obtained with a field-dependent permittivity model for the water layer. The effect of the electric field cannot be neglected because at high field strengths, relative permittivity is a strong function of electric field[25]. The field distribution for a field-dependent relative permittivity can be found by solving Laplace's and Poisson's equations numerically, as described previously[2]. The relative permittivity of the water was allowed to vary between low and high field limits of 80 and 2, respectively, with the transition occurring between

0.01 and 1 V/Å. The potential distribution was found using the Newton-Raphson method to solve Poisson's equation for the water layer and Laplace's equation for the vacuum.

The model predicts that the field is concentrated at the tip-water and water-vacuum interfaces. Fig. 8 shows the dependence of constant electric field lines on water thickness and applied electric field. The predominant field is predicted to be at the water-vacuum interface in thin water layers. As the water thickness increases, the field at the vacuum interface decreases and the field at the tip surface increases for a given applied field. When the water becomes sufficiently thick, the location of the predominant field shifts to the tip-water interface. The left-hand curve in Fig. 8 represents the locus of points where the field at the water-vacuum interface F_v is 0.4 V/Å while the right-hand curve represents the same for the field at the tip-water interface F_t. The curves in Fig. 8 are for a field of 0.4 V/Å, but the trends are the same at other field strengths. Ionization begins when either F_v or F_t becomes sufficiently large. As illustrated in Fig. 8, ionization is expected to begin at the vacuum interface in thin layers and at the tip surface in thick layers.

3. Permittivity Model Comparison

The trends predicted by the constant and variable permittivity models are the same: as the water thickness increases the tip field increases and the vacuum field decreases for a given applied field. Fig. 9 compares the predicted tip and vacuum fields as a function of water thickness for a constant permittivity of 65 (the solid lines) and the variable permittivity model (the symbols). The value of the constant permittivity was selected because it provided the best match with the variable permittivity results. The vacuum field predictions for both models agree with each other. There is a slight deviation between the two models near $x = 0.5$ because the average permittivity

of the numerical model is slightly less than 65 for very thin layers. The agreement between the two models implies that the vacuum field is dependent upon average relative permittivity in the water layer.

The tip field predictions in Fig. 9 compare well with each other for thin layers, but strongly diverge for thicker layers. The agreement of the variable permittivity prediction with the constant permittivity prediction for thin layers is not surprising because the field, and therefore the permittivity, will be relatively constant in thin layers. The predictions diverge for thick water layers because the tip field strongly depends upon the local value of permittivity and its rate of change at the tip surface, and is less dependent upon the average permittivity. As a result of this dependence, the numerical model predicts that the tip field will be amplified (i.e., larger than the applied field) in very thick layers. Note that the predicted trend of the dominance of F_v vs. F_t does not depend upon permittivity model: F_v dominates in thin layers and F_t dominates in thick layers for both permittivity models.

Field-induced reactions will occur at locations where the electric field is at a maximum. Therefore, for a water covered emitter tip, the field-induced reaction should occur at either the tip surface or the vacuum interface. Positive ions formed at the vacuum interface will be ejected from the water layer when they are created, as shown in Fig. 10a. This implies that the onset of ionization is not influenced by the negative ions that are left in the adlayer. Positive ions formed at the tip surface, on the other hand, must migrate through the adlayer and then desorb from the surface before they can be detected, as shown in Fig. 10b. Thus, ions will be present in the water layer before they are detected in our measurements. A key assumption in the numerical model is that no ions are present in the adlayer. Clearly, this is not true when ionization occurs at the tip

surface and, as a result, the numerical model is not expected to accurately predict the onset of ionization in thick layers.

Both the constant and variable relative permittivity models predict that there is a critical thickness x_c below which the vacuum field dominates and above which the tip field dominates. Above the critical thickness ionization should occur at the tip surface and below x_c ionization should occur at the vacuum interface. Eqn. 13 predicts that the critical thickness will decrease with decreasing relative permittivity. As mentioned above, the average permittivity in thin layers is lower for the variable permittivity model. Therefore, the critical thickness predicted by the variable permittivity model should be less than the critical thickness for the constant permittivity model. The critical thickness of the curves in Fig. 9 are 6.0 and 7.1 for the variable permittivity and constant permittivity models, respectively.

If the ionization mechanism does change at the critical thickness, then the RFD experimental results should be distinctly different for thin and thick layers. Several RFD experimental results indicate that thin layers are ionized by a different mechanism than thick layers: (1) ionization images of thin and thick layers are different, (2) plots of onset field as a function of ice thickness (Fig. 1) have a critical thickness at which the data changes slope, and (3) ionization onset is independent of ramp rate in thin layers but dependent upon ramp rate in thick layers. Ionization independent of ramp rate is consistent with ionization at the vacuum interface and ionization dependent upon ramp rate is consistent with ionization at the tip surface because positive ions formed at the vacuum interface will be ejected from the water when they are created and those formed at the tip surface will require a finite amount of time to diffuse through the water and desorb from the surface, as shown in Fig. 10. Therefore, the data are consistent with

the model predictions. Given the validity of the proposed ionization mechanisms, it is instructive to examine the implications of these mechanisms on ionization at the vacuum interface and tip surface.

B. Ionization at the Vacuum Interface (Thin Layers)

The numerical model predicts that ionization occurs at the vacuum interface in thin water layers. Fig. 8 shows that in the limit of zero thickness, the applied field F_o is the same as the field at which water ionizes at the vacuum interface F_v. From Fig. 1, F_v is 0.27 V/Å at 143 K. Values for F_v as a function of temperature are shown in Fig. 5.

The heavy line in Fig. 1 is the trend predicted by the variable permittivity model for F_v = 0.27 V/Å. The predicted trend agrees well with the experimental data. The best way to evaluate the numerical model is to compare the predicted and measured values of $dF_{app,o}/dx$ because the vacuum field (i.e., the y-intercept of Fig. 8) was determined from the experimental data. The slope $dF_{app,o}/dx$ is a function of the vacuum field F_v, dimensionless thickness x, and the permittivity ε (Eqn. 10). The predicted temperature dependence of the slopes is shown by the solid lines in Fig. 3. The discontinuity in the solid lines is due to the step change that occurs in the ionization field at 130 K (see Fig. 5). The predicted slopes are within the error of the experimentally obtained slopes for thin, crystalline layers, however, the predicted slopes are considerably higher than the measured slopes for amorphous layers.

One possible explanation for the ability of the numerical model to predict the field distribution in crystalline layers, but not in amorphous layers, is that the dielectric properties are different. Fig. 2 compares the predicted thickness dependence with that determined from the

RFD data at 108 K. The predicted slope is five times larger than the measured slope. Eqn. 10 shows that the predicted slope can be decreased by increasing the relative permittivity ε. Line *d* in Fig. 2 is the predicted trend when ε is infinite. The measured trend falls well below this line. Therefore, the observed differences in the measured and predicted slopes for amorphous water do not seem to be due to dielectric properties.

The other explanation for the difference between the predicted and measured slopes is that the amorphous adlayer changes shape in the presence of an applied field, i.e., the amorphous phase is mobile. Three phases of water exist below 160 K: an amorphous solid, a highly viscous fluid, and a crystalline solid. Both the amorphous and crystalline solids are immobile [10,16]. The highly viscous fluid, on the other hand, is capable of large scale translational motion between the glass transition temperature and the point at which the sample completely crystallizes[16,17].

If the water layer is mobile, then it may not be uniform (Fig. 11a), as assumed in the numerical model. The shape of the water layer will be determined by the interaction of two opposing forces: those due to surface tension and those due to the potential gradient. Surface tension forces will tend to thin the water layer at the tip. In the presence of an applied field, the potential gradient will act upon the dipole of the water and push it toward the tip apex. If the surface tension forces are larger than the forces due to the applied field, then the water layer will thin, as shown in Fig. 11b. Line *b* in Fig. 2 (the dashed line) shows that the thickness of the experimental data would need to be reduced by a factor of 5 to match the prediction. Conversely, if the forces due to the applied field predominate, then the fluid will form a small drop or cone at the apex, as shown in Fig. 11c. In this case, the ionizing field is larger than would be inferred from the applied field. Line *c* in Fig. 2 shows how the data would need to be adjusted for this

case. This line is diagonal because both the water thickness and the field at the tip apex increase. The field near the apex will be enhanced because the water radius r_w is less than the tip radius r_t. Note that movement in either direction can explain the difference between the predicted and measured data. A mobile amorphous phase and an immobile crystalline phase could be the reason that the numerical model matches the experimental data for thin crystalline layers, but not thin amorphous layers.

C. Ionization at the Tip Surface (Thick Crystalline Layers)

Thick layers are defined as layers with dimensionless thicknesses x greater than the critical thickness. The critical thickness is the value of x at the slope break in plots of onset field and thickness (e.g., Fig. 1). As discussed above, the numerical model is not expected to predict the field distribution in thick layers because ions will be present in the water layer before they are detected (Fig. 10b). Nonetheless, based on the success of the numerical model for thin crystalline layers, it is tempting to use the model to estimate the ionization field at the tip surface for thick crystalline layers. As shown in Fig. 1, the breakpoint at 143 K occurs at $x = 0.52$ and $F_{app,o} = 0.40$. The predicted tip field at these conditions is 0.0079 V/Å, nearly two orders of magnitude lower than the ionization field at the vacuum interface. This difference may be due not only to ions in the water, but also because our model assumes that the field is uniform over the tip surface and neglects interactions between the tip and the ice layer. The water molecules near the tip surface will be preferentially aligned with the tip surface, decreasing the relative permittivity near the tip and increasing the value of the tip field. Clearly, a molecular level model that more accurately simulates the system is needed to predict the value of the tip field.

As shown in Fig. 1, the slope of the thick coverage line in the RFD experiments was

positive. The numerical model and Eqn. 12 predict that the slope of the thick coverage line should be negative (for $\varepsilon > 1$). A positive slope does not rule out ionization at the tip surface because the applied field at which the ions are detected may not be the field at which they were formed. An ion formed at the tip surface must travel through the ice layer, desorb from the surface, and travel to the phosphor screen before it can be detected (Fig. 10b). The ramp rate dependence of the ionization onset field (Fig. 7) indicates that this process takes a finite amount of time and is therefore diffusive in nature. Diffusive ion transport depends upon ion hydration effects, as previously noted for transport of F^- through H_2O films[26]. Ionization at the vacuum interface, on the other hand, should be independent of ramp rate because the ions will be ejected from the surface when they are formed (Fig. 10a). As shown in Figs. 6 and 7, the trends observed in the ramp rate studies are consistent with the proposed mechanism: ionization in thin layers is independent of ramp rate and ionization in thick layers is linearly dependent upon ramp rate at low rates.

In thick layers the applied field at ionization onset plateaus at higher ramp rates. This plateau may be due to ionization at the vacuum interface that is enhanced by the presence of positively charged ions in the ice layer. Positive ions created at the tip surface will be repelled from the positively charged surface and migrate towards the vacuum interface. This excess positive charge in the water layer increases the electric field at the vacuum interface and reduces the applied field needed for ionization at that interface. The ramped field desorption data are consistent with the hypothesis that ions are present in the adlayer, because the applied fields at the plateau are considerably less than the predicted applied fields needed to ionize water at the vacuum interface. For example, at 108 K the vacuum field for ionization is 0.50 V/Å. The

numerical model predicts that at $x = 2.9$ the applied field will need to be 2.3 V/Å when ionization begins at the vacuum interface, yet the data in Fig. 6 plateaus at 1.0 V/Å at $x = 2.9$.

If the first ions detected at low ramp rates originated at the tip surface, then extrapolation of the ramp rate data to zero ramp rate should give the value of the applied field at which the ions began to form at the tip surface. At 143 K and $x = 2.4$ the extrapolated onset field is 0.36 V/Å. This point was extrapolated using the best fit line (Fig. 7) through the low ramp rate data because the data in this region is linear. This point is the filled triangle in Fig. 1. The extrapolated onset field is less than the onset fields for most of the data; only data at coverages less than $x = 0.45$ have onset fields less than 0.36 V/Å. If it is assumed that ionization at the tip surface begins at the breakpoint and that the filled triangle represents the applied field at ionization onset at $x = 2.4$, then the dashed line in Fig. 1 is the line of constant tip field. This line has a slope of –0.02 V/Å, which is negative as expected. Ramp rate data at additional thicknesses are needed to verify this trend.

The ramp rate data in Figs. 6 and 7 for thick ice layers show that the onset of ionization in amorphous ice is less sensitive to changes in electric field than ionization onset in crystalline ice. In the RFD experiments, temperature is held constant and ionization is solely due to an increase in the polarization energy provided by the electric field. The polarization energy, E_p, is defined as

$$E_P = \mu F + \alpha F^2 / 2 \approx \mu F , \tag{14}$$

where μ is the dipole moment and α the polarizability. The polarizability term in Eqn. 14 is small at the fields used in this work. Eqn. 14 shows that the magnitude of the dipole moment controls the sensitivity of polarization energy to the electric field. As a result, a larger applied field will be

required to initiate ionization when the dipole moment is small. Therefore, the ramp rate data indicate that the dipole moment of amorphous ice layers is less than the dipole moment of crystalline layers. This observation is in agreement with the estimated the dipole moments for amorphous and crystalline ice of 3.9 Debye and 5.1 Debye, respectively[4].

The relative permittivity of the water adlayer at the thickness of the slope break can be estimated using Eqn. 13 from the critical thickness data in Fig. 4, where

$$\varepsilon = (x_c + 1)^2. \tag{15}$$

The estimated values of the relative permittivity are shown on the second y-axis of Fig. 4. The average relative permittivity is ~10 for the amorphous phase and ~2.5 for the crystalline phase. These results are somewhat surprising because the relative permittivity is directly proportional to the product of the dipole moment and density[25]. Both the dipole moment[4] and the density[23] are lower for amorphous ice than for crystalline ice. The estimated relative permittivity for amorphous ice may be too large due to field-induced movement of amorphous ice away from the tip apex prior to ionization onset. If this occurs, then the estimated permittivity for amorphous ice is too high because the values of x_c used in Eqn. 13 were too large. In the previous section it was estimated that the layer thins by a factor of 5, as a result, the estimated permittivity for amorphous ice should be 2.05. This is in excellent agreement with the permittivity measured by Tsekouras et. al.[27].

V. CONCLUSIONS

The ionization of water layers adsorbed under field-free conditions depends upon the thickness of the water. Both variable and constant permittivity models predict that thin water

layers ionize at the vacuum interface and that thick layers ionize at the tip surface. The trends measured in our ramped field desorption experiments are consistent with the model predictions. Data for thin, crystalline layers match the predicted trends. The inability of the model to predict the trends in thin, amorphous layers has been attributed to adlayer mobility. The most likely direction of movement is toward the tip shank, which will decrease the water thickness at the tip apex. The numerical model is not expected to predict trends in thick layers due to the presence of ions in the water layer, but ramp rate studies provide evidence that ionization in thick layers occurs at the tip surface. Ramp rate studies also qualitatively show that the dipole moment of amorphous ice is less than the dipole moment of crystalline ice. The estimated relative permittivity for crystalline ice is 2.5 and that of amorphous ice is 2.05.

ACKNOWLEDGEMENTS

We gratefully acknowledge support of this work from the Office of Naval Research.

REFERENCES

1 D. M. Kolb and C. Franke, *Appl. Phys. A* **49,** 379 (1989).

2 D. L. Scovell, T. D. Pinkerton, B. A. Finlayson, and E. M. Stuve, *Chem. Phys. Lett.* **294,** 255-261 (1998).

3 A. Stintz and J. A. Panitz, *Surf. Sci.* **296,** 75-86 (1993).

4 D. L. Scovell, T. D. Pinkerton, and E. M. Stuve, *Surf. Sci.* (submitted).

5 D. S. Olander and S. A. Rice, *Proc. Nat. Acad. Sci. USA* **69,** 98-100 (1972).

6 A. H. Narten, C. G. Venkatesh, and S. A. Rice, *J. Chem. Phys.* **64,** 1106-1121 (1976).

7 T. C. Sivakumar, S. A. Rice, and M. G. Sceats, *J. Chem. Phys.* **69,** 3468 (1978).

8 W. Hagen, A. G. G. M. Tielens, and J. M. Greenberg, *Chem. Phys.* **56,** 367-379 (1981).

9 N. J. Sack and R. A. Baragiola, *Phys. Rev. B* **48,** 9973-9978 (1993).

10 W. C. Simpson, M. T. Sieger, T. M. Orlando, L. Parenteau, K. Nagesha, and L. Sanche, *J. Chem. Phys.* **107,** 8668-8677 (1997).

11 P. Lofgren, P. Ahlstrom, D. V. Chakarov, J. Lausmaa, and B. Kasemo, *Surf. Sci.* **367,** L19-L25 (1996).

12 G. P. Johari, A. Hallbrucker, and E. Mayer, *J. Chem. Phys.* **95,** 2955-2964 (1991).

13 M. Sugisaki, H. Suga, and S. Seki, *Bull. Chem. Soc. Jpn.* **41,** 2591 (1968).

14 J. A. McMillan and S. C. Los, *Nature* **206,** 806 (1965).

15 A. Hallbrucker, E. Mayer, and G. P. Johari, *J. Phys. Chem.* **93,** 7751 (1989).

16 R. S. Smith and B. D. Kay, *Surf. Rev. Letters* **4,** 781-797 (1997).

17 P. Jenniskens, S. F. Banham, D. F. Blake, and M. R. S. McCoustra, *J. Chem. Phys.* **107,** 1232-1241 (1997).

18 L. Onsager, D. L. Staebler, and S. Mascarenhas, *J. Chem. Phys.* **68,** 3823-3828 (1978).

19 T. D. Pinkerton, D. L. Scovell, A. L. Johnson, B. Xia, V. K. Medvedev, and E. M. Stuve, *Langmuir* **15,** 851-856 (1999).

20 T. Sakurai, A. Sakai, and H. W. Pickering, *Atom-Probe Field Ion Microscopy and its Applications* (Academic Press, Inc., Boston, 1989).

21 T. T. Tsong, *Atom-Probe Field Ion Microscopy* (Cambridge University Press, Cambridge, 1990).

22 R. Gomer, *Field Emission and Field Ionization* (Harvard University Press, Cambridge, 1961).

23 D. E. Brown, S. M. George, C. Huang, E. K. L. Wong, K. B. Rider, R. S. Smith, and B. D. Kay, *J. Phys. Chem.* **100,** 4988-95 (1996).

24 A. Stintz and J. A. Panitz, *J. Appl. Phys.* **72,** 741-5 (1992).

25 H. P. Huinink, A. deKeizer, F. A. M. Leermakers, and J. Lyklema, *J. Phys. Chem.* **100,** 9948-9954 (1996).

26 M. Akbulut, T. E. Madey, and P. Nordlander, *J. Chem. Phys.* **106,** 2801-10 (1997).

27 A. A. Tsekouras, M. J. Iedema, and J. P. Cowin, *Phys. Rev. Letters* **80,** 5798-5801 (1998).

Captions

Fig. 1. Applied field at ionization onset as a function of deposited ice thickness x at 143 K. The heavy line is a prediction by the numerical model for a vacuum field F_v of 0.27 V/Å. The solid circles are thin coverage data and the open circles are thick coverage data. The thin line is a least squares fit of the thick coverage data. The triangle is the extrapolated value of the ionization onset field at zero ramp rate for $x = 2.5$. The shaded rectangles are the measured range in the ramp rate data shown in Fig. 7.

Fig. 2. Comparison of measured and predicted trends in ionization onset as a function of thickness at 108 K. Line *a* is the predicted trend for a constant water thickness. Line *b* shows the correction needed to the data if the water layer thins during an experimental run. The plot shows how much thinning of the water layer is needed to match the prediction. Line *c* is the correction needed if the forces exerted by the applied field deform the water layer. Line *d* is the prediction for infinite permittivity of the water layer.

Fig. 3. Temperature dependence of the slope of the thin coverage line. The open circles are the measured data and the solid lines are the theoretical data. Water below 130 K is amorphous and above 130 K it is crystalline.

Fig. 4. Temperature dependence of the thickness at the slope break, or critical thickness, x_c. The dashed line is a guide to the eye. The value of ε was estimated from Eqn. 15.

Fig. 5. Temperature dependence of the field F_v required to ionize thin water layers. F_v is the same as the ionization onset field in the limit of zero thickness, F_o. This field was determined by the y-intercept in plots similar to Fig. 1. The solid and dashed lines are least squares fits of the data below and above 130 K, respectively.

Fig. 6. Effect of changes in the ramp rate of the applied field for ionization onset at 108 K for dimensionless thicknesses of 0.7, 2.9, and 4.3. The solid lines are least squares fit of the data (on a linear plot), and the dashed lines are extrapolated.

Fig. 7. Effect of changes in the ramp rate of the applied field at 143 K for dimensionless thicknesses of 0.6 and 2.4. The solid lines are least squares fit of the data (on a linear plot), and the dashed lines are extrapolated.

Fig. 8. Lines of constant vacuum field F_v and tip field F_t of 0.4 V/Å as a function of dimensionless thickness x. The dashed line is the thickness at which the ionization mechanism is expected to change. In thin layers ionization is expected to occur at the vacuum interface and in thick layers it is expected to occur at the tip surface.

Fig. 9. Comparison of predicted values of the vacuum field F_v and the tip field F_t for an applied potential of 100 V and a tip radius of 200 Å. The symbols are the predictions for the variable permittivity model, and the lines are the predictions for a constant permittivity of 65.

Fig. 10. Schematic of the ionization process at (a) the water-vacuum interface and (b) at the tip surface. The heavy lines represent the interface where ionization occurs.

Fig. 11. Water covered emitter tips. (a) Emitter tip covered by a constant thickness of water. (b) Deformation in water layer when surface tension forces predominate. (c) Deformation in the water layer when forces due to the applied electric field predominate. Note that the radius of the water r_w is less than the tip radius r_t.

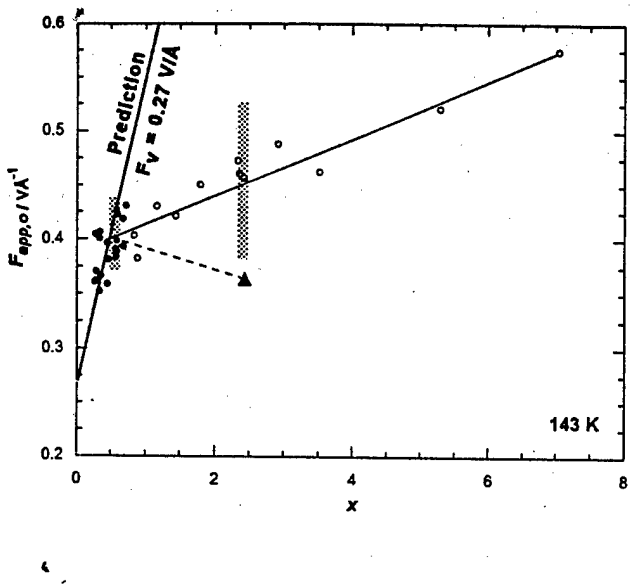

Fig. 1
Scovell, et. al.

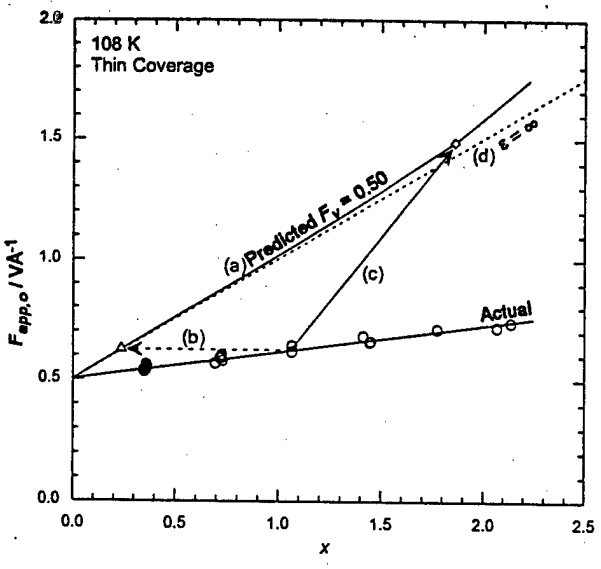

Fig. 2
Scovell, et. al.

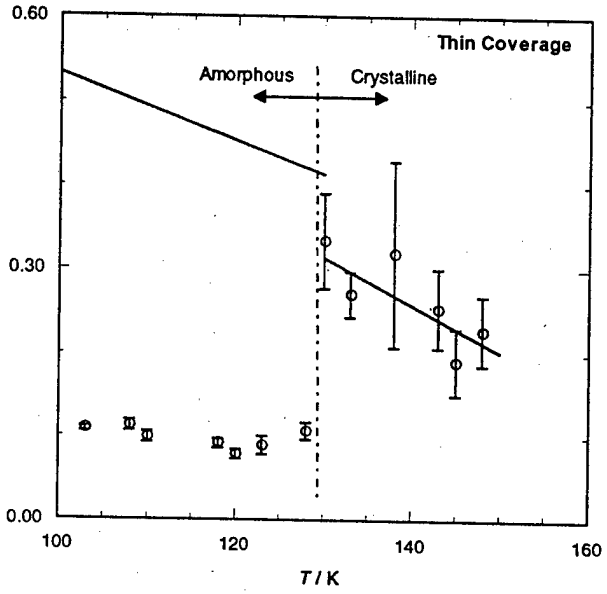

Fig. 3
Scovell et. al.

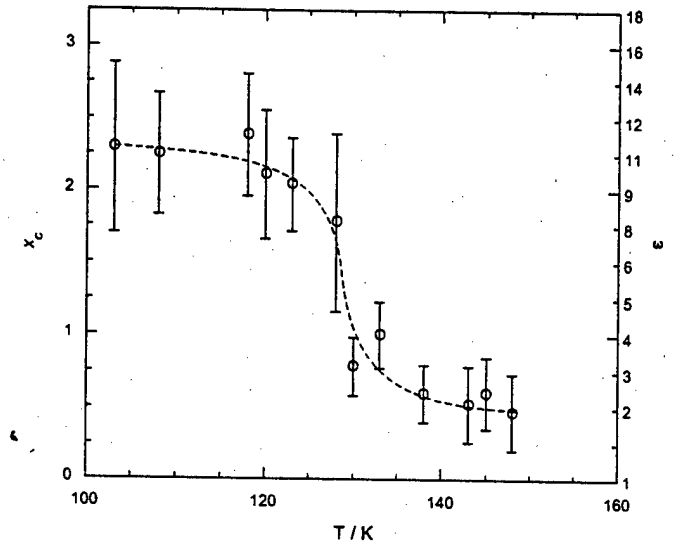

Fig. 4
Scovell et. al.

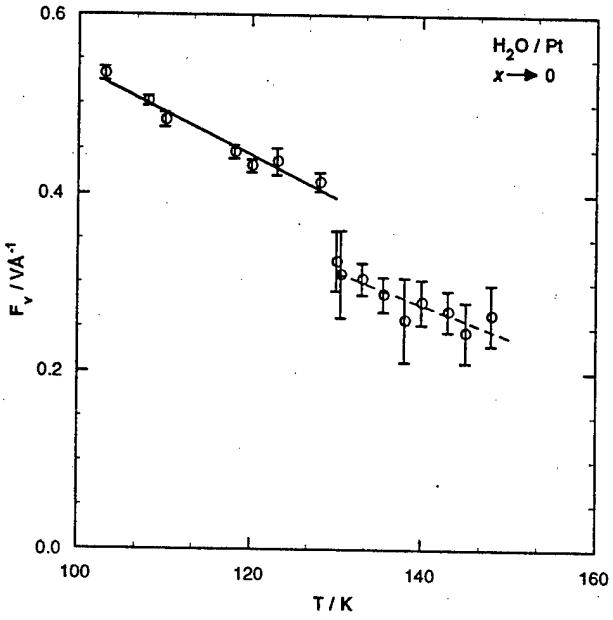

Fig. 5
Scovell et. al.

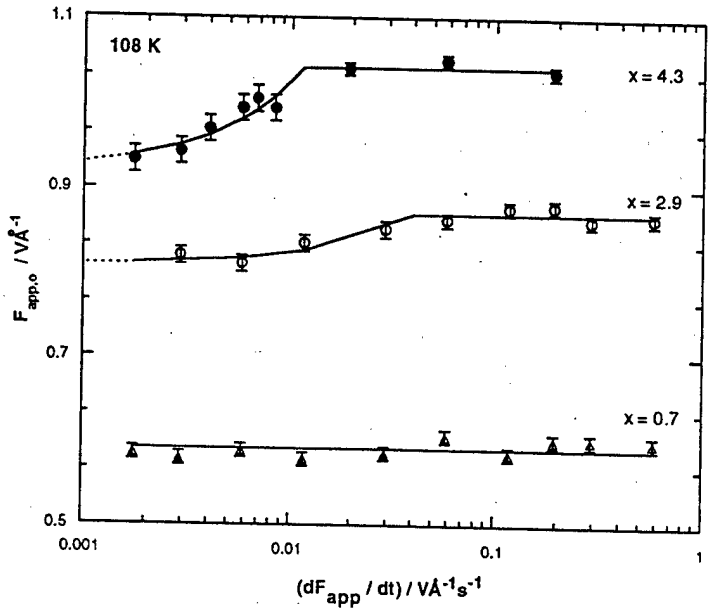

Fig 6
Scovell, et. al.

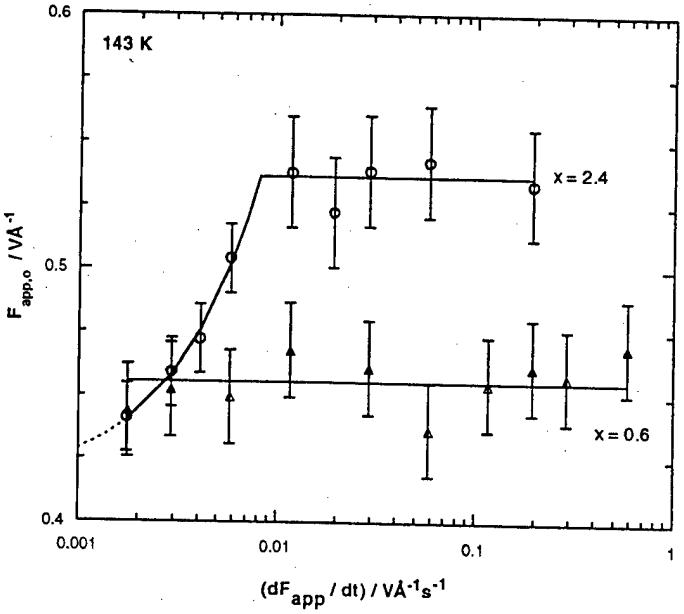

Fig 7
Scovell, et. al.

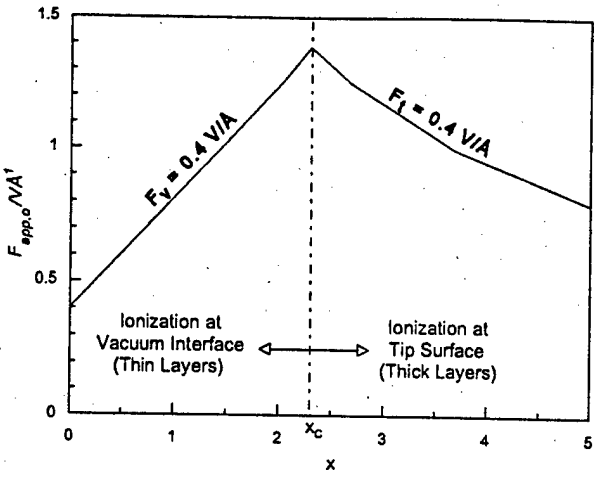

Fig. 8
Scovell, et. al.

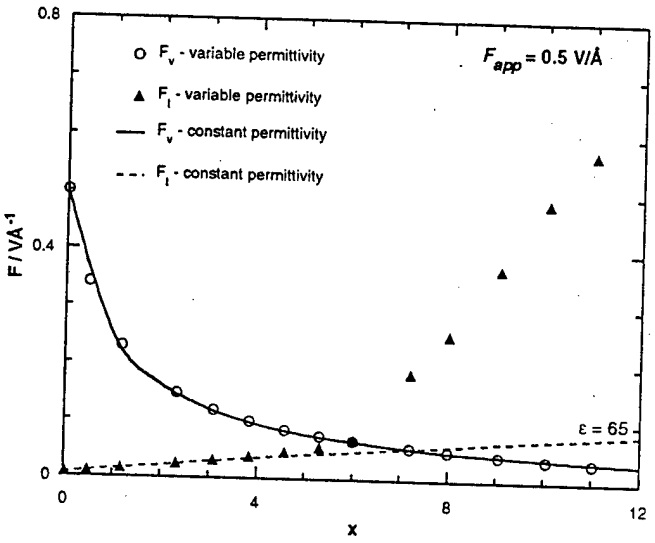

Fig. 9
Scovell, et. al.

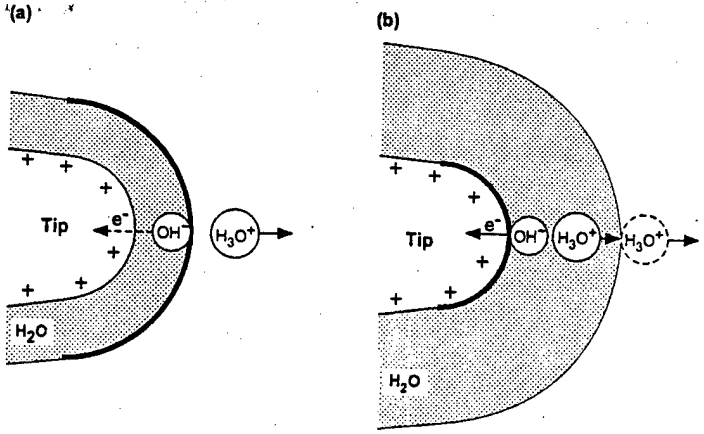

Fig. 10
Scovell, et. al.

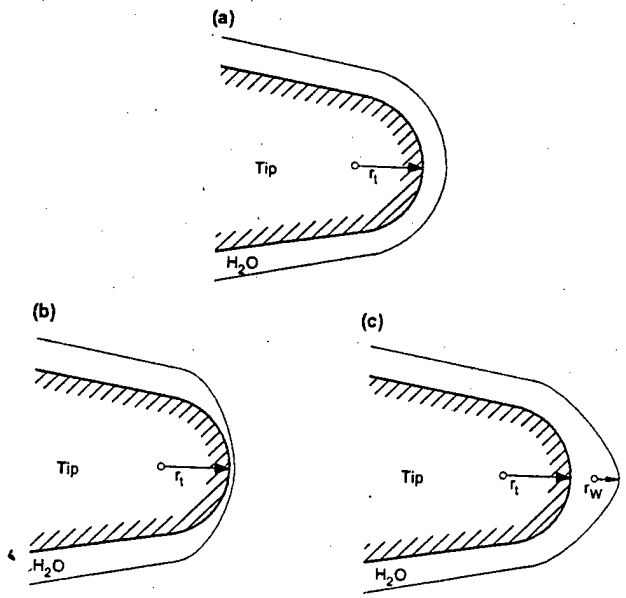

Fig. 11
Scovell, et. al.